Inorganic Chemistry

pubs.acs.org/IC

Article

^{59}Co Thermal Sensitivity in Co(III) Trisdithiocarbamate Complexes

Ökten Üngör,[‖] Sara Termos,[‖] Robert W. Schurko,* and Joseph M. Zadrozny*

Cite This: *Inorg. Chem.* 2025, 64, 6531−6543

Read Online

ACCESS | Metrics & More | Article Recommendations | Supporting Information

ABSTRACT: Understanding temperature sensitivity in magnetic resonance is key to novel molecular probes for noninvasive temperature mapping. Herein, we report an investigation of the effects of heavy-donor-atom dithiocarbamate ligands on the variable-temperature ^{59}Co nuclear magnetic resonance (NMR) properties of six Co(III) complexes: Co(et_2-dtc)$_3$ (**1**), Co(bu_2-dtc)$_3$ (**2**), Co(hex_2-dtc)$_3$ (**3**), Co(pyrr-dtc)$_3$ (**4**), Co(benzyl$_2$-dtc)$_3$ (**5**) and Co(2,6-dmpip-dtc)$_3$ (**6**) (et_2-dtc = diethyldithiocarbamate; bu_2-dtc = dibutyldithiocarbamate; hex_2-dtc = dihexyldithiocarbamate; pyrr-dtc = pyrrolidine-dithiocarbamate; benzyl$_2$-dtc = dibenzyldithiocarbamate; and 2,6-dmpip-dtc = 2,6-dimethylpiperidine-dithiocarbamate). This study reveals ^{59}Co chemical-shift temperature dependences of 1.17(3)−1.73(4) ppm/°C as a function of ligand substituents. Solid-state Raman spectroscopic analyses show that more Raman-active Co−S_6 vibrational modes correlate to higher thermal sensitivities for these compounds, in line with our current model for temperature sensitivity. Short spin−lattice relaxation T_1 times in solution (*ca.* 200 μs) were observed, and correlation with T_2* times and solid-state ^{59}Co NMR analyses reveal that the solution-phase line widths are attributable to quadrupolar relaxation processes, which ultimately lower temperature-sensing resolution.

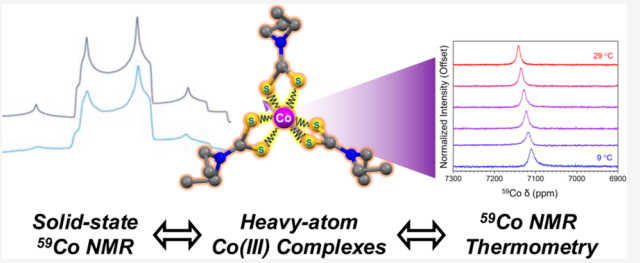

INTRODUCTION

Magnetic resonance thermometry is a promising method for noninvasive temperature mapping in vivo.[1−4] This capability can be harnessed for monitoring the progress of thermal ablation during tumor treatment,[5,6] or unveiling the intricate mechanisms of thermal management within the body, which consistently reveals new insights.[7]

Cobalt-59 nuclear spins are particularly promising for temperature detection via magnetic resonance due to the notable temperature sensitivity of the ^{59}Co nuclear magnetic resonance (NMR) chemical shift (δ), $\Delta\delta/\Delta T$.[8,9] A recent report by us shows that ^{59}Co set records for temperature sensitivity in air-sensitive (up to $\Delta\delta/\Delta T$ = 150 ppm/°C)[10] and air-stable species ($\Delta\delta/\Delta T$ = 3.50 ppm/°C).[11] Understanding how to amplify sensitivities beyond these levels in air-stable species remains remains vital for imaging applications. Hence, continued focus on fully low-spin octahedral Co(III) complexes which are stabilized by the d^6 ligand field stabilization energy.

Our group recently reported a synthetic design goal for high-temperature sensitivity ^{59}Co NMR based on vibrations.[12−14] In this design strategy, a molecule with more lower-energy Raman (or symmetric) vibrations exhibits a chemical shift with a higher temperature sensitivity. We used this hypothesis to create molecules with asymmetric acac-like ligands that elevated the benchmark for the sensitivity of air-stable, octahedral, low-spin Co(III) nuclei up to 3.50 ppm/°C in Co(accp)$_3$.[11] This value is larger than that of the structurally similar Co(acac)$_3$, which held the record at 3.15 ppm/°C for a closed-shell species for four decades.[11]

The success of the foregoing design strategy suggests that even larger temperature sensitivities will result from a complex that has even more lower-energy Raman-active vibrations. In this context, ligands with heavy donor atoms are immediately of interest, as an increased donor atom mass should lower the fundamental frequencies of any M−L vibrations and increase $\Delta\delta/\Delta T$ (Figure 1). However, despite the existence of many variable-temperature NMR studies of ^{59}Co, as well as basic studies of heavy-atom donors on chemical shift and nuclear-spin relaxation,[15−18] none have studied the role of heavy donor atoms on the temperature dependence of the ^{59}Co δ.

Herein, we provide the first test of how ligand S-donor atoms control ^{59}Co $\Delta\delta/\Delta T$ by examining a series of six octahedral cobalt tris(dithiocarbamate) complexes: Co(et_2-dtc)$_3$ (**1**), Co(bu_2-dtc)$_3$ (**2**), Co(hex_2-dtc)$_3$ (**3**), Co(pyrr-dtc)$_3$ (**4**), Co(benzyl$_2$-dtc)$_3$ (**5**) and Co(2,6-dmpip-dtc)$_3$, and (**6**) (et_2-dtc = diethyldithiocarbamate; bu_2-dtc = dibutyldithiocarbamate; hex_2-dtc = dihexyldithiocarbamate; pyrr-dtc = pyrrolidine-dithiocarbamate; benzyl$_2$-dtc = dibenzyldithiocarbamate; and 2,6-dmpip-dtc = 2,6-dimethylpiperidine-dithio-

Received: December 17, 2024
Revised: March 10, 2025
Accepted: March 20, 2025
Published: March 27, 2025

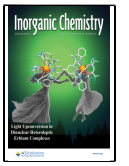

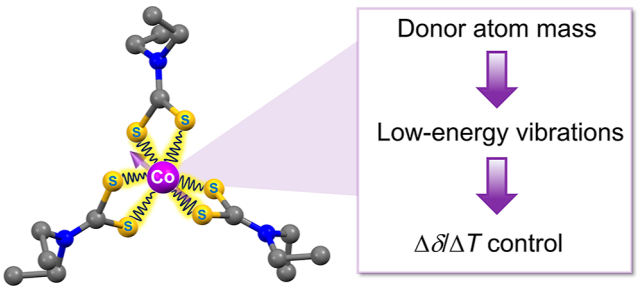

Figure 1. This paper investigates the effects of heavy donor atoms on ^{59}Co chemical-shift temperature sensitivity. The crystal structure of the example complex Co(et_2-dtc)$_3$ is taken from ref 36. Purple, yellow, blue, and gray spheres correspond to cobalt, sulfur, nitrogen, and gray spheres, respectively, with hydrogen atoms omitted for clarity.

carbamate). These molecules can be categorized into two subgroups: **1**−**3** vary in the size of the alkyl functional groups on the ligands, while **4**−**6** vary cyclic and aromatic groups attached to the dithiocarbamate core. A comparative analysis of the temperature dependence of the ^{59}Co chemical shifts and Raman spectra of **1**−**6** reveal unexpectedly lower temperature dependence than expected, suggesting that the temperature-dependence of ^{59}Co NMR signals is not governed by ligand mass alone. Furthermore, we performed SSNMR measurements of ^{59}Co chemical shift anisotropy (CSA) and electric field gradient (EFG) parameters for **1**−**6** and three Co(acac)3-like complexes, as well as solution ^{59}Co T_1 measurements. These latter experiments reveal new insight into ^{59}Co spin relaxation mechanisms of **1**−**6**, which contribute to the thermometry resolution trends for these species.

EXPERIMENTAL SECTION

General Considerations. Complex **1** was synthesized following the procedure outlined in the previous report.[19] Compounds **2**−**6** were synthesized with minor adjustments to this procedure. Sodium diethyldithiocarbamate trihydrate (Na(et_2-dtc)·3H_2O), dibutylamine, dihexylamine, pyrrolidine, dibenzyl amine, and 2,6-dimethylpiperidine were purchased from Sigma-Aldrich. Their purity was confirmed via ^{1}H NMR before use. Sodium dithiocarbamate salts of dibutylamine,[20] dihexylamine,[20] pyrrolidine,[21] and dibenzylamine[22] were prepared using established literature methods. Co(acac)$_3$ (**A**) was used as received from Sigma-Aldrich, Co(tBu-acac)$_3$ (**C**) was used as received from Thermo Fischer Scientific, and Co(accp)$_3$ (**B**) was prepared by literature methods.[11] ***Caution***! Carbon disulfide (CS_2) was handled exclusively in a fume hood with nitrile gloves and safety goggles due to its volatility, flammability, and toxicity, and all waste was collected in sealed solvent waste containers. Except the use of CS_2, no uncommon hazards are noted. All reactions were carried out under air.

*Co(et_2-dtc)$_3$ (**1**).* The synthesis of complex **1** was accomplished according to the previously reported method.[19] A solution of Na(et_2-dtc)·3H_2O (1500 mg, 8.8 mmol) in 10 mL of warm deionized water (DI H_2O) and a solution of $CoCl_2$·6H_2O (500 mg, 2.1 mmol) in 10 mL of DI H_2O are prepared separately. The ligand solution was carefully introduced into the cobalt solution, leading to the formation of a dense and green precipitate. To facilitate the oxidation of Co(II) to Co(III), 4 mL of 30% (w/w)H_2O_2 solution was slowly added. We note that the product was still obtained in the absence of H_2O_2. The resulting mixture was stirred for an additional 15 min until all effervescence ceased, indicative of a complete reaction. The green powder was collected by vacuum filtration and washed with 10 mL of cold ethanol and dried under vacuum for 30 min (965 mg, 91.4% yield) ^{1}H NMR (δ, 400 MHz, $CDCl_3$): 1.29(t, 18H, CH_3), 3.64(q, 12H, CH_2), 3.82(m) ppm; ^{13}C NMR (δ, 400 MHz, $CDCl_3$): 14.77, 42.00, 210 ppm. Anal. Calcd (Found) for $C_{15}H_{30}CoN_3S_6$: 35.77 (35.27) % C, 8.34 (8.00) % N and 6.00 (5.77) % H. UV−vis (CH_2Cl_2, 1 mM, Figure S1) $\lambda_{max,}$ nm (ε_M, M^{-1} cm^{-1}): 247(60), 269(85), 321(34) and 639(81). IR and Raman spectra and their analysis are presented in the main text and Supporting Information. These data are consistent with the prior report.[19]

*Co(bu_2-dtc)$_3$ (**2**).* The compound was prepared in the same manner as for **1** from sodiumdibutyldithiocarbamate (718 mg, 3.1 mmol) and $CoCl_2$·6H_2O (500 mg, 2.1 mmol); **2** was isolated as a green powder; 925 mg, 65.5% yield. ^{1}H NMR (δ, 400 MHz, $CDCl_3$): 0.92(t, 18H, CH_3), 1.32(m, 12H, CH_3−CH_2), 1.52(m, 12H, CH_2) 2.98(m, 12H, CH_2−S) ppm; ^{13}C NMR (δ, 400 MHz, $CDCl_3$): 212, 52.46, 25.30, 14.00 ppm. Anal. Calcd (Found) for $C_{27}H_{54}CoN_3S_6$: 48.26 (48.00) % C, 6.25 (5.95) % N and 8.10 (7.89) % H. UV−vis (CH_2Cl_2, 1 mM, Figure S1) λ_{max}, nm (ε_M, M^{-1} cm^{-1}): 248(12), 273(29), 324(24) and 647(62). IR and Raman spectra and their analysis are presented in the main text and Supporting Information.

*Co(hex_2-dtc)$_3$ (**3**).* The compound was prepared in the same manner as for **1** from sodium dihexyldithiocarbamate (878 mg, 3.1 mmol) and $CoCl_2$·6H_2O (262 mg, 1.1 mmol). Recrystallization from $CHCl_3$ yielded solid green powder **3**; 510 mg, 55.2% yield. ^{1}H NMR (δ, 400 MHz, $CDCl_3$): 0.90 (t, 18H, CH_3), 1.32 (m, 12H, CH_3−CH_2), 1.67 (m, 24H, CH_2), 3.45−3.79 (m, 24H, CH_2−S) ppm; ^{13}C NMR (δ, 400 MHz, $CDCl_3$): 204.87, 48.59, 31.46, 27.20, 26.58, 22.61, 14.03 ppm. Anal. Calcd (Found) for $C_{39}H_{78}CoN_3S_6$·0.2$CHCl_3$: 54.48 (54.92) % C, 4.86 (5.10) % N and 9.11 (8.81) % H. UV−vis (CH_2Cl_2, 1 mM, Figure S1) λ_{max}, nm (ε_M, M^{-1} cm^{-1}): 252(92), 272(48), 322(70) and 639(130). IR and Raman spectra and their analysis are presented in the main text and Supporting Information.

*Co(pyrr-dtc)$_3$ (**4**).* The compound was prepared in the same manner as for **1** from sodium pyrrolidinedithiocarbamate (525 mg, 3.1 mmol) and $CoCl_2$·6H_2O (262 mg, 1.1 mmol); **4** was isolated as a green powder; 420 mg, 76.7% yield. ^{1}H NMR (δ, 400 MHz, $CDCl_3$): 1.32 (m, 12H, CH_2), 1.44 (m, 6H, N−CH_2), 3.68−3.94 (t, 6H, CH_2−S) ppm; ^{13}C NMR (δ, 400 MHz, $CDCl_3$): 206.20, 44.40, 29.45, 22.40, 13.55 ppm. Anal. Calcd (Found) for $C_{15}H_{24}CoN_3S_6$: 36.20 (36.13) % C, 8.44 (8.36) % N and 4.86 (4.86) % H. UV−vis (CH_2Cl_2, 1 mM, Figure S1) λ_{max}, nm (ε_M, M^{-1} cm^{-1}): 277(63), 325(35), 453(161) and 650(137). IR and Raman spectra and their analysis are presented in the main text and Supporting Information.

*Co(dibenzyl-dtc)$_3$ (**5**).* The compound was prepared in the same manner as for **1** from sodium dibenzyldithiocarbamate (1862 mg, 6.3 mmol) and $CoCl_2$·6H_2O (500 mg, 2.1 mmol); **5** was isolated as a green powder; 1515 mg, 82.4% yield. ^{1}H NMR (δ, 400 MHz, $CDCl_3$): 4.59 (d, 6H, CH_2−Ph), 5.13 (d, 6H, CH_2−Ph), 7.51 (m, 30H, aromatic) ppm; ^{13}C NMR (δ, 400 MHz, CDCl3): 209, 128.56, 125.50, 48.65 ppm. Anal. Calcd (Found) for $C_{45}H_{42}CoN_3S_6$: 61.69 (61.51) % C, 4.80 (4.85) % N and 4.83 (4.99) % H. UV−vis (CH_2Cl_2, 1 mM, Figure S1) λ_{max}, nm (ε_M, M^{-1} cm^{-1}): 264(94), 314(72), 349(127) and 625(95). IR and Raman spectra and their analysis are presented in the main text and Supporting Information.

*Co(2,6-dmpip-dtc)$_3$ (**6**).* The compound was prepared in situ by reacting $CoCl_2$·6H_2O (238 mg, 1 mmol) in 5 mL of DI H_2O and a mixture of 2,6-dimethylpiperidine (339 mg, 3 mmol) and CS_2 (228 mg, 3 mmol) in 5 mL of DI H_2O The reaction mixture was stirred for 2 h at room temperature and then filtered, yielding dark green powder. 338 mg, 50.5% yield. ^{1}H NMR (δ, 400 MHz, $CDCl_3$): 1.20 (d, 18H, CH_3), 1.72 (m, 18H, ring CH_2/CH), 3.61 (s, 6H, N−CH_2) ppm; ^{13}C NMR (δ, 400 MHz, $CDCl_3$): 208, 44.78, 26.75, 15.50 ppm. Anal. Calcd (Found) for $C_{24}H_{42}CoN_3S_6$: 46.20 (45.87) % C, 6.74 (6.53) % N and 6.79 (6.47) % H. UV−vis (CH_2Cl_2, 1 mM, Figure S1) λ_{max}, nm (ε_M, M^{-1} cm^{-1}): 271(84), 312(148), 345(88) and 621(112). IR and Raman spectra and their analysis are presented in the main text and Supporting Information.

X-ray Data Collection, Structure Solution, and Refinement for 2. Single-crystal X-ray diffraction data were collected at the X-ray Diffraction facility of the Analytical Resources Core at Colorado State University. Data for **2** was collected at 110 K on a Bruker D8 Quest ECO single-crystal X-ray diffractometer equipped with Mo Kα (λ = 0.71073 Å). Data were collected and integrated using Bruker Apex 3 software. Absorption corrections were applied using SADABS.[23]

https://doi.org/10.1021/acs.inorgchem.4c05385
Inorg. Chem. 2025, 64, 6531−6543

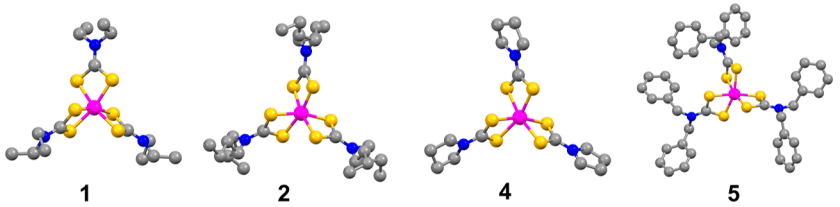

Figure 2. Crystal structures of the Co(III) complexes studied in this manuscript. Structures for **1**, **4**, and **5** are taken from previous reports.[36,37] H atoms are omitted for clarity. Color scheme; Co: magenta, S: yellow, N: blue, C: gray.

Space group assignments were determined by examination of systematic absences, E statistics, and successive refinement of the structures. Crystal structures were solved using SHELXT and refined with the aid of successive difference Fourier maps by SHELXL operated in conjunction with OLEX2 software.[24−26] Significant disorder was observed in the structure. Disorder in the butyl groups of the dithiocarbamate ligand shell in the structure of **2** were modeled with free variables. Carbon atoms in disordered alkyl chains were refined isotropically. Heavily disordered solvent, presumed MeCN, was present in the structure. A solvent mask was employed in the refinement to address this disorder and reported a total electron density consistent with one MeCN. Hydrogen atoms were placed in ideal positions and refined using a riding model for all structures. Crystal collection data are in Table S1 and the crystallographic information file for **2** is available in the CSD at accession number 2426923.

Variable-Temperature ^{59}Co NMR. Samples **1**−**6** were prepared as 0.7 mL volumes of 100 mM concentrations in CH_2Cl_2, $CHCl_3$, MeOH, and corresponding deuterated solvents. Spectroscopic measurements were made at a Larmor frequency, $\nu_0(^{59}Co)$, of 118.3 MHz using an Agilent Unity INOVA $\nu_0(^1H)$ = 500 MHz spectrometer at a field strength of 11.74 T with a 5 mm broadband NMR probe. Prior to measurement, the spectrometer was locked to the ^2H signal of a 1 M $K_3[Co(CN)_6]$ in D_2O standard to ensure that differences in resonances were not continually affected by a drifting magnetic field. Individual ^{59}Co chemical shifts are all referenced to $K_3[Co(CN)_6]$. ^2H locking for samples prepared with protonated solvents was accomplished by first, using a standard $CDCl_3$ sample to enable a ^2H lock, then second, this $CDCl_3$ sample was removed, the samples with Co(III) complex and protonated solvent was inserted, and finally the sample was measured by ^{59}Co NMR. In these cases, any error introduced to the spectrum from using the unlocked magnet can be converted to 0.1 Hz/h changes in the ^{59}Co NMR full-width at half-maximum (fwhm) line widths. Such deviations are negligible considering the 1−6 kHz (10−50 ppm) fwhm of the collected peaks. Variable-temperature measurements were made on each sample over 5−30 °C in 5 °C intervals. Temperature was controlled using a FTS Systems TC-84 Kinetics AirJet Temperature Controller to deliver a temperature-specific nitrogen stream directly to the probe and probe chamber. The temperature of the probe was monitored via thermocouple output. Temperature equilibration of the sample was allowed to occur over 15 min before the tuning and use of a 5 mm broadband probe for spectral collection. Inversion recovery experiments, performed with the same spectrometer and probe, were conducted on each sample at 25 °C. Inversion recovery data were acquired using 180°−τ−90° pulse sequence experiments with 180° and 90° pulse lengths set at 22.4 and 11.2 μs, respectively.

Solid-State ^{59}Co NMR. Prior to running SSNMR experiments, all samples were gently ground with a mortar and pestle and packed into 5 mm polychlorotrifluoroethylene (PCTFE) sample holders with Viton o-rings designed at the National High Field Magnetic Laboratory (NHMFL) in Tallahassee and produced by Shenzhen Rapid Direct Co, Ltd. ^{59}Co SSNMR experiments were run under stationary conditions (i.e., nonrotating samples) using Bruker NEO consoles on a 14.1 T/89 mm bore [$\nu_0(^1H)$ = 600 MHz, $\nu_0(^{59}Co)$ = 142.362 MHz] Bruker magnet and an 18.8 T/63 mm bore [$\nu(^1H)$ = 800 MHz, ν (^{59}Co) = 189.817 MHz] Oxford magnet at the NHMFL in Tallahassee. In-house built HX probes were used for all experiments. All samples were referenced to 1.0 M $K_3[Co(CN)_6]$ aqueous solutions with δ_{iso} (^{59}Co) = 0 ppm.[27,28] The Wideband Uniform-Rate Smooth-Truncation CPMG (WURST-CPMG) pulse sequence was used to acquire ultrawideline spectra.[29−33] A full listing of all experimental parameters for these measurements are provided in Tables S2−S13. Chemical shift tensor and EFG tensor parameters (Table S14) were extracted by simulations of the powder patterns using ssNake software,[34] which uses the $ZX'Z''$ convention for Euler angles; however, these angles were converted to the more common $ZY'Z''$ convention.[35]

Raman Spectroscopy. Raman spectra of **1**−**6** were collected at the Raman Microscopy Lab (RRID: SCR 019305) at the University of Colorado Boulder. Spectra were obtained using a Horiba LabRAM HR Evolution Spectrometer equipped with a 532 nm green laser (frequency-doubled Nd:YAG). Each of the dried compounds was measured as a powdered sample individually loaded onto glass slides. All spectra were collected between 100 and 650 cm^{-1} with the same spectral resolution utilizing 1800 gr/mm grating. Baseline subtraction and spectral deconvolution was performed in the Horiba LabSpec6 program.

All Other Characterization. ^1H and ^{13}C NMR spectra (in 50 mM solutions for ^{13}C NMR) of **1**−**6** dissolved in $CDCl_3$ were recorded on a Bruker Ascend 400 MHz spectrometer at 9.4 T ($\nu_0(^1H)$ = 400 MHz). UV−vis spectra were collected by using a Shimadzu UV-2600i UV−vis spectrophotometer. The spectra were recorded in 1 mM solutions of **1**−**6** in DCM at room temperature. Elemental analyses were performed by Robertson Microlit Analytical Testing Laboratories (Ledgewood, New Jersey, USA). Infrared spectra were recorded on a Nicolet 6700 FTIR spectrometer using a diamond window ATR.

RESULTS AND DISCUSSION

Syntheses and Molecular Structures. Compounds **1**, **4**, and **5** were synthesized based on the literature preparations,[19] and compounds **2**, **3**, and **6** were synthesized by slightly modifying these literature procedures. The crystallographic data for **1**, **4**, and **5** were previously reported[36,37] and **1**, **2**, **4**, and **5** are all shown in Figure 2. Single crystals of **2** were grown by slow evaporation from CH_2Cl_2, and **3**, in our attempts, did not yield single crystals suitable for diffraction.

Compounds **1**−**6** are all pseudo-octahedral, low-spin Co(III) complexes. Average Co−S bond distances range from 2.26(2) to 2.27(2) Å in **1**, **2**, **4**, and **5**, falling within the reported average distances for low-spin trivalent metal complexes with dithiocarbamates.[38−40] The average S−Co−S bite angle ranges from 85.6(3)° to 87.4(4)°, showing relatively minor variations, and the S−C bond distances are in the range of 1.713(3) to 1.735(6) Å. The C−N distances also vary slightly from 1.298(2) to 1.341(2) Å. All S_2CN units of the ligands are planar, hence the slight variations seen in C−N distances are not from distortions that break conjugation.

Continuous-Shape-Measurement analyses were also performed to check for geometrical structural trends.[41,42] If the structures of **1**−**6** matched an idealized octahedral O_h geometry, the resultant SHAPE score would be 0. Instead,

https://doi.org/10.1021/acs.inorgchem.4c05385
Inorg. Chem. 2025, 64, 6531−6543

the scores for **1**, **2**, **4**, and **5** are 1.62, 1.67, 1.55, and 1.79, respectively, indicating that all six compounds are distorted octahedral geometries, and the magnitudes do not follow any apparent trends connected to the identities of the ligand substituents.

Electronic Structures. We first studied the electronic structures of the cobalt(III) ions in **1**−**6** by electronic absorption spectroscopy. UV−vis absorption spectra of compounds **1**−**6** were measured in CH_2Cl_2 at room temperature (Figures 3a and S1). Under these conditions, all spectra

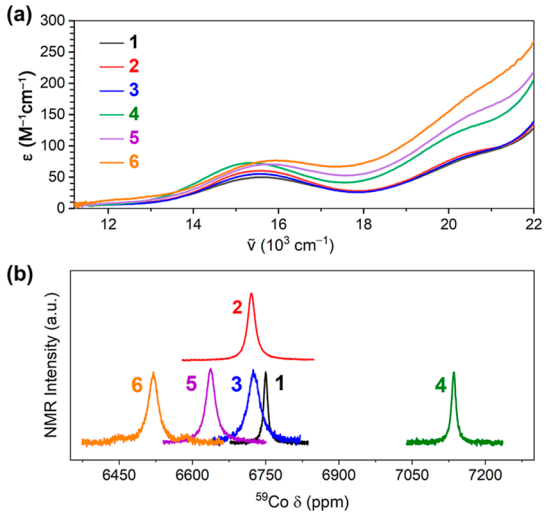

Figure 3. Characterization of Co(III) electronic structures in **1**−**6**. (a) UV−vis spectra for **1**−**4** in CH_2Cl_2 at room temperature, focused on the d−d transition. (b) ^{59}Co NMR spectra ($\nu_0(^{59}Co) \approx 118.3$ MHz) for **1**−**6** in $CDCl_3$ at room temperature. Spectra were collected using a 500 MHz ^{1}H/11.74 T magnet.

exhibit four different absorption bands, which is consistent with literature.[43−46] The molar absorptivity coefficients, ε_M, of *ca.* 100−200 M^{-1} cm^{-1} for the lowest-energy, 12,000−18,000 cm^{-1} peaks are consistent with their dark green colors in solution, likely arising from d−d transitions (i.e., $^1A_{1g}$ to $^1T_{1g}$ transition, following labels for O_h geometries).[47] The energies of the low-energy peaks and the d^6 Tanabe−Sugano diagram allowed us to quantify Δ_o, which increases from **4** (15,300 cm^{-1}) to **1** (15,400 cm^{-1}) to **2** (15,500 cm^{-1}) to **3** (15,600 cm^{-1}) to **5** (15,700 cm^{-1}) to **6** (15,800 cm^{-1}). In all, these values suggest generally weak ligand fields for the Co(III) ions, though not weak enough to enable high-spin ground states. Furthermore, the relative consistency in Δ_o across **1**−**6** is an effective control to preclude the possibility of substantial ligand field differences dictating the observed trends in $\Delta\delta/\Delta T$. Owing to the high ε values (>22,000 M^{-1} cm^{-1}), the higher energy bands can be assigned as either $\pi-\pi^*$ transitions from the S−C=S and N−C=S moieties of the dithiocarbamate ligand core (*ca.* 30,000−50,000 cm^{-1}),[48] or charge−transfer transitions (*ca.* 23,500−30,000 cm^{-1}).[49,50]

For all complexes, ^{59}Co NMR chemical shifts vary between 6500 and 7100 ppm (Figure 3b), in a similar range to those reported for sulfur-bound octahedral Co(III) complexes.[51−53] The chemical shift trend is **4** < **1** < **2** < **3** < **5** < **6**, in agreement with the lowest-energy peak in the UV−vis data (Figure 3a). More broadly, these observations are in agreement with prior results[15] and the larger established relationship between the energy of the $^1A_{1g}$ to $^1T_{1g}$ transition and the ^{59}Co δ in rigorous and distorted octahedral six-coordinate complexes.[9]

Variable-Temperature/Solvent ^{59}Co NMR Analyses. Variable-temperature ^{59}Co NMR spectra were recorded at 118.67 MHz with 100 mM solutions of **1**−**6** in $CDCl_3$ from 5 to 30 °C (Figures 4, S3−S9) using a 500 MHz/11.74 T NMR

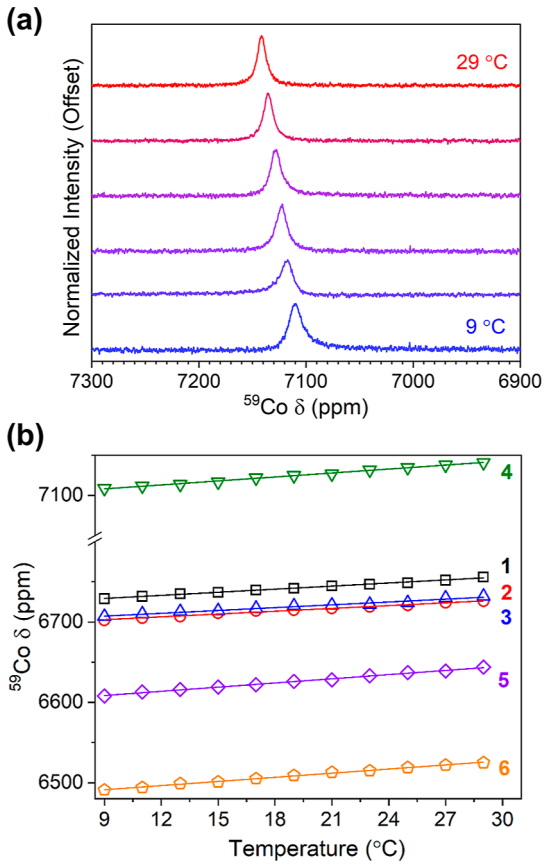

Figure 4. Variable-temperature ^{59}Co NMR data collected at 118.3 MHz. (a) Variable-temperature spectra collected for **4** from 9 to 29 °C (100 mM concentration in $CDCl_3$). (b) Comparison of temperature-dependent chemical shifts for **1**−**6**. Solid lines are linear regressions yielding $\Delta\delta/\Delta T$ values of 1.25(2), 1.18(3), 1.17(3), 1.65(4) 1.73(4) and 1.72(3) ppm/°C for **1**−**6**, respectively.

spectrometer. With increasing temperature, the ^{59}Co peaks for all complexes shift in a downfield direction to higher δ (i.e., in a high-frequency direction). Linear regression yields temperature sensitivities of 1.25(2), 1.18(3), 1.17(3), 1.65(4) 1.73(4) and 1.72(3) ppm/°C for **1**−**6**, respectively (Figure 4b, Table S15), or **3** ≈ **2** < **1** < **4** < **6** ≈ **5** in ranked order. These values are relatively small within the broader arena of complexes investigated with ^{59}Co variable-temperature NMR, which can have temperature sensitivities reaching up to 3.5 ppm/°C[11] for air-stable compounds and a maximum of 150 ppm/°C,[10] though significantly higher than the lowest known value of 0.15 ppm/°C for $Co(tBu_2acac)_3$ in CH_2Cl_2.[54]

Cobalt(III) complexes have chemical shifts that exhibit a solvent dependence,[54] and hence, we tested the matrix sensitivity of the ^{59}Co thermal responses of **1**−**6** through variable-solvent studies. We chose a range of solvents including $CHCl_3$, $CDCl_3$, CH_2Cl_2, toluene, pyridine, DMF, and 1,2-dichlorobenzene (DCB). These solvents were selected to account for variations in solubility across the series and well as

https://doi.org/10.1021/acs.inorgchem.4c05385
Inorg. Chem. 2025, 64, 6531−6543

the differences in solvent physical properties such as dielectric constant (from 2.38 to 36.71 for toluene to DMF, respectively[55]).[56] The ^{59}Co NMR peak and its temperature sensitivity differs slightly in each solvent (Figures S10–S15). The highest ^{59}Co $\Delta\delta/\Delta T$ values were observed for **2**, **4**, **5**, and **6** in $CDCl_3$ (Tables S16–S21) and 1.32(2) and 1.54(7) for **1** and **3** in $CHCl_3$. Otherwise, only slight changes (*ca.* 0.2–0.8 ppm/°C) were observed with variation in solvent identity and deuteration. Solvent-dependent $\Delta\delta/\Delta T$ values are found in Table S15 for **1**–**6**. We note that signal intensity dropped significantly for samples with concentrations lower than 100 mM; therefore, concentration dependence could not be assessed accurately. The limited characterization of the solvent-dependent NMR properties of compound **6** is due to its low solubility. Finally, the present data show only small changes in the ^{59}Co chemical shift with solvent donor properties (Figures S16 and S17), suggesting a lack of conventional solvent–solute interactions (e.g., H-bonding[13]) as a controlling factor for $\Delta\delta/\Delta T$.

Spin–Lattice Relaxation Analyses. We measured the spin–lattice relaxation times (T_1, also known as the longitudinal relaxation time) for **1**–**6** as a starting point to assess if and how the S_6 ligand fields control ^{59}Co nuclear-spin relaxation. For T_1, inversion recovery experiments were performed on 100 mM solutions at temperatures of 10 and 25 °C. We performed these experiments in different solvents as well to analyze temperature- and solvent-dependent behavior of T_1. The recovery curves are given in Figures S18–S28. The T_1 data for **1**–**6** reveal that T_1 lengthens with rising temperature: T_1 ranges (in $CDCl_3$) extend from 228(9) to 292(8) μs for **1**, 120(5) to 150(2) μs for **2**, 63(1) to 103(6) μs for **3**, 193(5) to 276(6) μs for **4**, 95(2) to 115(3) μs for **5**, and 163(3) to 222(4) μs for **6** from 10 to 25 °C (Figures S18–S28). This behavior is consistent with all of the molecules undergoing isotropic tumbling in the extreme narrowing limit (ENL), i.e., correlation times, $\tau_c \lesssim 10^{-11}$ s.[57] A listing of the T_1 data is in Table S22. At a cursory level, the effects of T_1 times appear to be reflected in the ^{59}Co peak line widths. Complexes **1** and **4**, with the longest T_1 values, have the narrowest ^{59}Co NMR peaks, whereas **2**, **3**, and **5** exhibit shortest T_1 times and broadest signals. These trends generally hold across solvents, with some exceptions (Table S22).

The observed T_1 values for **1**–**6** are shorter than homoleptic octahedral cobalt(III) complexes with six N- or O-coordinated ligands, which typically fall within the millisecond range.[58] The spin–lattice relaxation of the ^{59}Co nucleus is often attributed to nuclear electric quadrupolar coupling interactions, determined by the symmetry and structure of the ligand shell.[59] Departure away from spherical or Platonic symmetry about the quadrupolar nucleus most often corresponds to an increased quadrupolar interaction,[60,61] and hence, increased relaxation rates; hence, the six-coordinate, distorted octahedral Co(III) environments likely have large quadrupolar interactions, a conclusion that is underlined by the solid-state NMR analyses (vide infra).

^{59}Co NMR Line Width Analyses and T_2* Relaxation Times. We conducted line width analyses of the observed ^{59}Co peaks for **1**–**6** in various solvents and as a function of temperature (Figures 5a, S29–S34). In $CDCl_3$ at 25 °C, ^{59}Co NMR peaks for **1**–**6** are all relatively broad with full width at half-maximum values ($\nu_{1/2}$) of 9.65, 18.40, 29.76, 10.72, 22.70, and 25.04 ppm, respectively, which correspond to frequencies of 1.14, 2.17, 3.51, 1.27, 2.68, and 2.95 kHz, respectively.

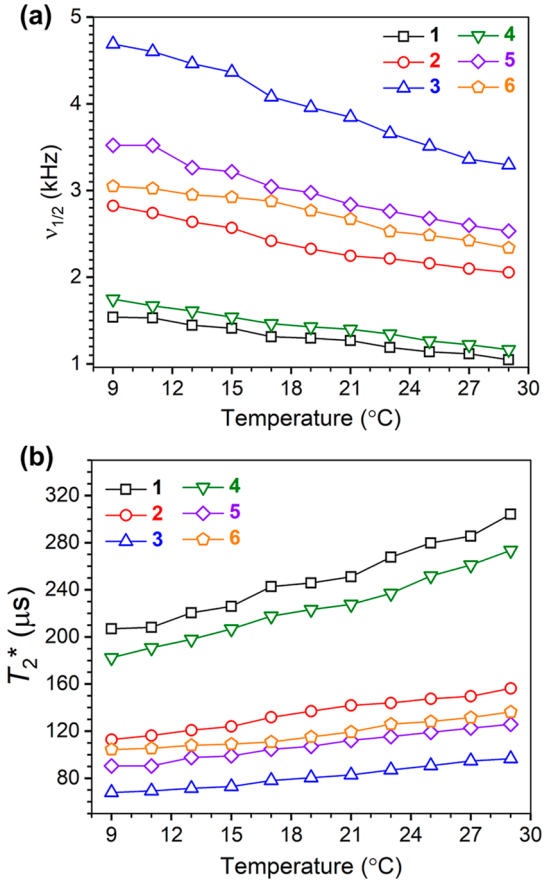

Figure 5. (a) ^{59}Co NMR line width values (in units of kHz) for **1**–**6** as a function of temperature in $CDCl_3$. (b) Temperature dependence of T_2* values for **1**–**6** calculated using resonance line widths. The solid lines are guides for the eye.

These broad line width values increase as the temperature decreases for all complexes (Figure 5a), again consistent with isotropic tumbling in the ENL. Across all complexes, we observe significant changes in line width when changing solvents. Conversely, in DCB, except for compound 2 in pyridine, we observed the broadest ^{59}Co NMR peaks. In DCB at 25 °C, the order of increasing fwhm values was as follows: **4** < **2** < **1** < **5** < **3**.

The ^{59}Co NMR line width contains information about the effective T_2 (T_2*) values of **1**–**6**, which account for both the natural T_2 and peak broadening from magnetic field inhomogeneities, i.e., $T_2^{*-1} = T_2^{-1} + T_{inh}^{-1}$. We extracted these T_2* values from the temperature-dependent NMR line widths using the relationship $T_2^* = 1/(\pi\nu_{1/2})$, where $\nu_{1/2}$ (in kHz) represents the line width at the full width at half-maximum (fwhm) of the ^{59}Co NMR peak. Importantly, due to the rapid relaxation of these molecules, we were unable to directly measure T_2 values via experimental methods like Hahn-echo or CPMG experiments with our available instrument. Hence, these line width measurements, which are conducted upon peaks that are predominantly broadened by quadrupolar relaxation effects, are our best measure of relaxation dynamics. The temperature-dependent trends in T_2* for all complexes are illustrated in Figure 5b (also Figures S35–40). In general, complexes **1**–**6** exhibit an increasing T_2* with rising temperature. The longest T_2* values are observed in CH_2Cl_2, and complexes **1** and **4** exhibit the longest T_2* values

https://doi.org/10.1021/acs.inorgchem.4c05385
Inorg. Chem. 2025, 64, 6531–6543

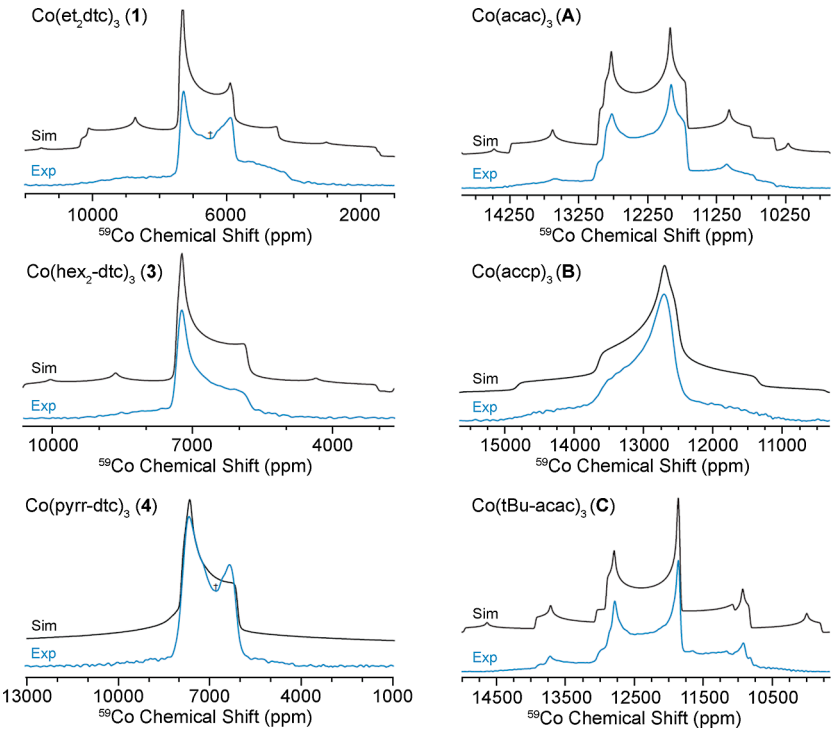

Figure 6. ^{59}Co SSNMR powder patterns (in blue) acquired at 18.8 T using the CPMG sequence for the Co−S_6 series, i.e., (**1**) Co(et_2-dtc)$_3$, (**3**) Co(hex_2-dtc)$_3$, and (**4**) Co(pyrr-dtc)$_3$, and the WURST-CPMG sequence for Co−O_6 series, i.e., (**A**) Co(acac)$_3$, (**B**) Co(bzac)$_3$, and (**C**) Co(*t*Bu-acac)$_3$. Numerical simulations of the spectra are shown in black. †Indicates magic-angle dips, see text for details.

among **1**−**6**. Slight increases (*ca.* 30 μs) in T_2* for all complexes are observed with solvent deuteration based on a comparison of $CDCl_3$ and $CHCl_3$. DCB appeared unique in all respects, in that T_2* values for **1**−**6** were notably shorter, by *ca.* 140 μs compared to the other solvents, which is very likely due to its comparatively high viscosity (vide infra, see Table S23).

Importantly, the measured T_2* values are all very close to the T_1 values under a given set of conditions. For example, T_1 for **1** at 10 and 25 °C in $CDCl_3$ is 228 and 292 μs, respectively, while T_2* values under these same conditions are 208 and 279 μs. This close correspondence between T_1 and T_2* follows all the measurements we report for **1**−**6** in different solvents and temperatures (Tables S22−S24 and Figure 5, S35−S36). The value of T_1 imparts a limit on the magnitude of T_2* (i.e., $T_1 \geq T_2$*), as is the case for **1**−**6**. Hence, a deeper understanding of the longitudinal relaxation mechanisms is required if we are to understand their impacts on temperature sensitivity for **1**−**6** (vide infra), which ultimately necessitated solid-state NMR measurements.

Solid-State NMR Analyses. The T_1(^{59}Co) and T_2(^{59}Co) relaxation constants for **1**−**6** have their origins in NMR interactions such as the chemical shift anisotropy (CSA) and quadrupolar interaction (QI). These anisotropic interactions do not result in time-independent manifestations in solution NMR spectra (i.e., shifts, splittings, and/or inhomogeneous patterns); however, they have mechanisms that drive longitudinal and transverse nuclear magnetic relaxation of nuclides like ^{59}Co. In the ENL of motion, the longitudinal relaxation rate, $R_1 = 1/T_1$, and the transverse relaxation rate, $R_2 = 1/T_2$, are proportional to the square of their interaction constants. For QI, the rates scale proportional to the square of quadrupolar coupling constant, C_Q^2, and for the CSA, the rates scale proportional to the approximate square of span, Ω^2 (in Hz) (vide infra).[57] In theory, it is possible to determine the magnitudes of the interaction constants from measurements of T_1 or T_2 in solution, but in practice, this is very challenging due to a number of approximations that must be made (especially regarding the correlation time, τ_c, as well as temperature, concentration, viscosity, etc., vide infra).

Alternatively, SSNMR can accurately quantitate the anisotropic NMR interactions via measurement of the chemical shift (CS) and electric field gradient (EFG) tensors (for the CSA and QI, respectively), since they manifest as inhomogeneously broadened patterns in SSNMR spectra. Together, this information and solution-phase NMR relaxation time constants enable (1) the calculation of correlation times, (2) elucidation of dominant relaxation mechanisms, and (3) yield insights into the elements of molecular structure that dictate these tensors and the concomitant relaxation properties. Note that this analysis assumes similarity between molecular structure in the solid and solution phases. For coordination compounds that are diluted in an NMR solvent, this is most often the case, unless there are solvent interactions that substantially alter the molecular structure of the compound in question.[62,63] This approximation seems to be valid for **1**−**6**, since variations in T_1 and T_2* in different solvents are observed, but represent differences of less than an order of magnitude in each case. Furthermore, the effects of solvent viscosity track exactly with the corresponding T_1 values, with less viscous solvents resulting in the highest T_1 values, and corresponding decreases in T_1 at lower temperatures (see Table S23)—these observations indicate that coordination of solvent molecules are unlikely to have a significant effect on the magnitude of the quadrupolar interaction and concomitant relaxation parameters.

Understanding all of the foregoing factors can lead to the rational design of cobalt complexes that are favorable for molecular thermometers, such as those with tunable T_1 and T_2

https://doi.org/10.1021/acs.inorgchem.4c05385
Inorg. Chem. 2025, 64, 6531−6543

constants and/or anisotropic interactions that are highly dependent upon temperature and/or viscosity. In this light, it is of great value to compare the ^{59}Co NMR interaction tensor parameters and ^{59}Co relaxation time constants of the Co−S_6 series reported herein to those determined for Co(III) complexes with asymmetric acac-like ligands, dubbed here as the Co−O_6 series, as these are otherwise the highest-thermal-sensitivity ^{59}Co NMR thermometers in air-stable Co(III) complexes.[11]

Although ^{59}Co (I = $^7/_2$) has a natural abundance of 100% and a receptivity with respect to ^{13}C of R_C = 1635.29, the acquisition of SSNMR spectra is challenging, due in part to the sizable inhomogeneous broadening resulting from the CSA and QI. The second-order quadrupolar interaction (SOQI) and CSA dominate central transition patterns (CT, $\pm$ $^1/_2$ ↔ $\pm$ $^1/_2$), while both these and the first-order quadrupolar interaction impact the satellite transitions (ST; $\pm$ $^1/_2$ ↔ $\pm$ $^3/_2$, $\pm$ $^3/_2$ ↔ $\pm$ $^5/_2$, $\pm$ $^5/_2$ ↔ $\pm$ $^7/_2$).[64] For higher spin half-integer quadrupolar nuclides (I = $^7/_2$, $^9/_2$), the ST patterns have significant overlap with the narrower, high intensity CT patterns—this overlap can lead to severe distortions in certain powder patterns, making the acquisition of uniform powder patterns a challenge. Moreover, careful choice of excitation and refocusing powers to minimize powder pattern distortions in spin echo experiments need consideration.[27,65,66]

^{59}Co SSNMR spectra were acquired using the WURST-CPMG pulse sequence[29,31−33] under static conditions at 14.1 and 18.8 T for Co−S_6 compounds (**1**), (**3**), and (**4**), as well as the Co−O_6 series, Co(acac)$_3$ (**A**), Co(accp)$_3$ (**B**), and Co(tBu-acac)$_3$ (**C**) (see Figures 6, S41, and S42). We note that the WURST-CPMG sequence can produce artifacts known as "magic-angle dips" in very broad patterns like those of the Co−S_6 series; however, it is still possible to extract relatively accurate sets of anisotropic NMR interaction tensor parameters from simulations.[66−70]

The CT patterns in the ^{59}Co SSNMR spectra of the Co−S_6 series are influenced by the effects of both CSA and SOQI. Numerical simulations yield values of C_Q of 11.5, 15, and 21 MHz for **1**, **3**, and **4**, respectively, with corresponding η_Q values of 0.35, 0.50, and 0.95 (Table S14). The δ_{iso} values are in the range of 6700−7300 ppm, which are consistent with solution NMR values. The spans of the CS tensors, Ω, are found to range from 1500 to 1800, with positive skews, κ, ranging from 0.75 to 0.85, indicating that δ_{33} is the distinct component of the CS tensor in each case. The Euler angles, β, range from 0° to 10°, indicating that the directions of the principal components of the CS and EFG tensors, δ_{33} and V_{33}, respectively, are closely aligned. This is consistent with the pseudo-C_3 symmetry of the Co−S_6 units in the crystal structures of **1** and **4** (there is no structure for **3**); hence, these components should be aligned along/near their pseudo-C_3 axes. The uncertainties in the NMR interaction tensor parameters are relatively high, since (i) there are broad ST patterns underlying the CT patterns, which can cause distortions,[27] and (ii) the influences of the SOQI and CSA on the powder pattern are comparable in magnitude. These two factors make spectral acquisition and simulation challenging, unlike for many of the ^{59}Co SSNMR spectra reported in the literature, which often feature dominant manifestations of either the SOQI or CSA in the CT patterns (i.e., $\omega_Q \gg \omega_0\Omega$ or $\omega_Q \ll \omega_0\Omega$).[27,28,71]

The ^{59}Co SSNMR spectra of the Co−O_6 series **A**, **B**, and **C**, are distinct from those of the Co−S_6 series. First, the CT patterns are significantly narrower, with simulations indicating C_Q values ranging between 5.0 and 6.0 MHz. The η_Q values for **A** and **C** are low, indicating EFG tensors of higher axial symmetry than for the Co−S_6 series. The larger value of C_Q and increased η_Q value for **B**, in comparison to those of **A** and **C**, are consistent with symmetry differences revealed by the crystal structures (i.e., **B** is an asymmetric propeller with C_3 symmetry whereas **A** and **C** are pseudosymmetric propellers with approximate D_3 symmetry; the former is further departed from O_h symmetry).[11] The δ_{iso} values, which range from 12,000 to 13,000 ppm, are much higher than those of the Co−S_6 series, and also consistent with solution NMR data. The Ω values are similar to those of Co−S_6; however, the κ values are negative (between −0.60 and −0.95), which indicates that the δ_{11} are the distinct CS tensor components. This is consistent with the β that are close to 90°, which indicates that δ_{11} and V_{33} are closely aligned, and likely along the pseudo-C_3 axes. Comparison of these two sets of spectra reveals that the effects of ^{59}Co CSA on the CT patterns are far more dominant for the Co−O_6 series. Furthermore, for the spectra of **A** and **C**, well-defined, underlying ST patterns are observed that can be simulated with high precision, whereas for those of **B**, only a trace of the ST patterns is observed. Another useful comparison between **A**, **B**, and **C** involves the effective T_2 in the solid state, T_2^{eff}, which is the natural T_2 that arises from *all* contributions including quadrupolar, CSA, and mostly decoupled heteronuclear dipolar mechanisms. The measured T_2^{eff} for **B**, in this case measured with WURST-CPMG experiments (vide infra), is much lower than those of **A** and **C**, as indicated by the much shorter CPMG echo trains of the former, and concomitant reduction in S/N (Table S24 and Figures S41−S48). This behavior likely indicates an increased contribution to the T_2^{eff} in **B** from quadrupolar relaxation mechanisms (measurements of T_2^{eff}(^{59}Co) are provided in Table S24).

A number of comprehensive studies have been published over the last 40 years that describe ^{59}Co nuclear relaxation mechanisms for small molecules in solution with motions in the ENL.[58,59,72−79] ^{59}Co nuclear relaxation in six-coordinate cobalt complexes can be influenced by CSA, quadrupolar, scalar, dipolar, and/or spin-rotation mechanisms. The total longitudinal relaxation rate, R_1, can be expressed as the sum of the relaxation rates from each mechanism

$$R_1 = T_1^{-1} = R_1(\mathrm{CSA}) + R_1(\mathrm{Q}) + R_1(\mathrm{SC}) + R_1(\mathrm{SR}) + R_1(\mathrm{DD}) \quad (1)$$

For ^{59}Co, contributions from CSA and quadrupolar mechanisms are often found to be the most dominant. In the ENL, R_1(Q) and R_1(CSA) can be expressed as

$$R_1(\mathrm{Q}) = T_1^{-1}(\mathrm{Q}) = \frac{3\pi^2}{10} C_Q^2 \left(1 + \frac{n_Q^2}{3}\right)\left(\frac{2I+3}{I^2(2I-1)}\right)\tau_c \quad (2)$$

$$R_1(\mathrm{CSA}) = T_1^{-1}(\mathrm{CSA}) = \frac{2}{15}\gamma^2 B_0^2 \Omega^2 \tau_c \quad (3)$$

where γ is the gyromagnetic ratio and B_0 is the external magnetic field. Note that Ω is often given as $\Delta\delta$ or $\Delta\sigma$, where the CS tensor is assumed to be axially symmetric, with κ = ± 1.[57]

https://doi.org/10.1021/acs.inorgchem.4c05385
Inorg. Chem. 2025, 64, 6531−6543

Measurements of T_1 and T_2 constants for the Co−S_6 and Co−O_6 series from solution NMR spectra reveal that those of the former complexes are generally at least 3 orders of magnitude smaller than those of the latter (Tables S24−S25). Hence, the SSNMR data indicates that larger C_Q values in the Co−S_6 series are responsible for these differences, consistent with the results of modern ^{59}Co solution NMR studies on Co(acac)$_3$ and other octahedral Co(III) complexes.[58,59,63,72,73,77,79] Again, this is under the well-supported premise that there are not large differences in the magnitudes in C_Q between the solid and solution phases (vide supra). To further investigate the relative contributions of ^{59}Co CSA and QI to T_1, we utilized values of τ_c for **A** in chloroform as reported by Kanakubo et al. ($\tau_c = 4.48 \times 10^{-11}$ s in a 220 mM solution of $CDCl_3$ at 298 K).[63] With this τ_c and the ^{59}Co tensor parameters from our SSNMR data (Table S14), quadrupolar and CSA relaxation rates were calculated using eqs 1 and 2, yielding $R_1(Q) = 573.5\ s^{-1}$ and $R_1(CSA) = 4.7\ s^{-1}$, for a total relaxation rate of $R_1 = R_1(Q) + R_1(CSA) = 578.2\ s^{-1}$. Therefore, $T_1 = 1.7$ ms, which is of the same order of magnitude as the T_1 of **A** in a 100 mM solution ($T_1 = 4.01$ ms)[12] reported in a previous paper. Assuming a similar τ_c, the relaxation rates for **1** are $R_1(Q) = 2484.2\ s^{-1}$ and $R_1(CSA) = 8.7\ s^{-1}$, respectively, leading to a $T_1 = 1/R_1 = 401\ \mu s$, which is also on the same order of magnitude as the T_1 value reported herein ($T_1 = 292\ \mu s$). We made analogous calculations for all of the remaining compounds, and similar results were found (Table S25).

The relatively small discrepancies between our predicted T_1 constants and those measured in solution confirm the value of having precise measurements of CS and EFG tensor parameters. In the absence of such information, assumptions about correlation times, solvent viscosities, solute−solvent interactions, and/or the tensor parameters, can lead to incorrect assumptions about the relative contributions of various mechanisms.[58,59,63,75,79−81] For example, for Co(acac)$_3$ in chloroform, the solvent viscosity was reported to decrease with increasing temperatures, which affects correlation times, and hence, affects relaxation rates in solution.[82] In addition, chloroform (used in this study) is known to form chelate complexes with M^{III}(acac)$_3$ species,[72,83,84] though we do not see evidence of this from our data. We would not expect that transient solute−solvent interactions should impact the values of C_Q to the degree that would cause relaxation differences of orders of magnitude. Finally, possible contributions of spin-rotation relaxation mechanisms were considered, since an instance of this has been reported for the bulky [Co(sepulchrate)]Cl$_3$ complex;[58] however, none of our solution ^{59}Co NMR measurements revealed that relaxation rates increased with increasing temperature, a hallmark of the spin-rotation relaxation mechanism.[57]

Vibrational Spectroscopic Analyses. Vibrational spectra of **1**−**6** were obtained using both IR and Raman spectroscopy. Solid-state FTIR spectra for **1**−**6** in the 400−4000 cm^{-1} region reveal a multitude of peaks. A discussion of their interpretation can be found in the Supporting Information (Figure S2). More broadly, while these vibrations are useful for general compound characterization, they do not provide useful insight into the temperature dependence based on current models.[14]

In contrast, Raman spectroscopy and symmetric vibrations are of explicit interest to understand ^{59}Co NMR temperature sensitivity. Hence, we used Raman spectroscopy to characterize **1**−**6** (Figure 7a). Note that Raman spectroscopy, at least

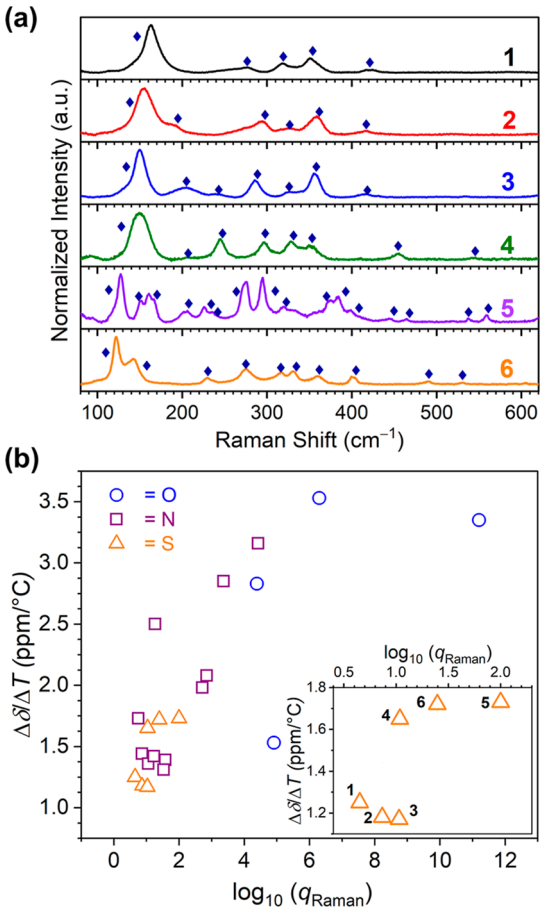

Figure 7. (a) Solid-state Raman spectra collected on **1**−**6**. Diamonds indicate peaks used for the calculation of q_{Raman} in part b. (b) Comparison of temperature sensitivity with calculated q_{Raman} values for **1**−**6** and other published reports. q_{Raman} values were computed using peaks identified in the experimental spectra. Data are clustered by donor atoms. Blue circles represent Co(III) complexes with O-donor atoms in the coordination shell, purple squares possess only N atom donors. **Inset:** zoom in of the data for **1**−**6**; each point is labeled with the relevant compound number.

compared to IR spectrometers, more readily measures the low-energy regime, <650 cm^{-1}, where Co−S stretches occur,[85−87] and can therefore better connect $\Delta\delta/\Delta T$ to vibrational properties. All complexes exhibit rich spectra with many peaks in this energy range. The most intense modes across all compounds were observed below 200 cm^{-1}. These modes take the form of either a single highly intense band (for **1**−**4**) or bands accompanied by shoulders (for **5** and **6**). These intense peaks are likely stretching modes of the dithiocarbamate moieties,[88−90] as Co−L stretches are expected within the 400−650 cm^{-1} range.[85−87] From **1**−**6**, the complexity of the spectra increase, which is observed in a straightforward manner as the number of peaks. Compounds **1**−**3**, exhibit 5, 6, and 7 peaks, respectively, while **4**, **5**, and **6** exhibited 8, 15, and 10 distinct bands below 650 cm^{-1}, respectively.

The foregoing data demonstrate that the mass of the donor atom has opposing effects on the change in $\Delta\delta/\Delta T$. Our previous studies suggested a correlation between the number of low-energy vibrations and higher $\Delta\delta/\Delta T$. Solid-state Raman spectroscopic analyses revealed that an increased number of Raman-active Co−S_6 vibrational modes correlates with higher thermal sensitivity in **1**−**6**, aligning with our current model for

https://doi.org/10.1021/acs.inorgchem.4c05385
Inorg. Chem. 2025, 64, 6531−6543

temperature sensitivity. However, when comparing sulfur-donor systems to those with oxygen- or nitrogen-donor atoms around the cobalt center, the trend differs. The scatter plot in Figure 7b illustrates the relationship between the logarithm of the q_{Raman} parameter versus the temperature dependence of the ^{59}Co NMR chemical shift. The q_{Raman} parameter was calculated based on the number of peaks and their corresponding energies in the Raman spectra. A clear trend emerges where oxygen-based systems exhibit the highest temperature sensitivity, followed by nitrogen-based systems, while sulfur-based systems consistently show the lowest sensitivity. This suggests that donor atom mass alone is not the sole determining factor influencing temperature sensitivity; rather, a more complicated combination of vibrational characteristics and the coordination environment likely play a role in governing this behavior.

DISCUSSION

Proposed Origin of Low Temperature Sensitivity. The motivating hypothesis behind the present study was that heavier atoms would lower the energies of Raman-active vibrations, increase the vibrational partition function (q_{Raman}), and produce higher ^{59}Co thermal sensitivities. Surprisingly, the obtained q_{Raman} and $\Delta\delta/\Delta T$ values extracted from the Raman spectra and NMR data are all instead relatively low compared to other literature reports of ^{59}Co NMR thermometry. At the same time, within **1**−**6**, $\Delta\delta/\Delta T$ follows q_{Raman}. Hence, while our work shows that a higher temperature sensitivity does not simply follow from heavier donor atoms, the results from studying **1**−**6** fall in line with the general model for temperature sensitivity.

The spectroscopic data also contain two important disproofs of other mechanisms that may control temperature sensitivity. First, the work provides further evidence that ^{59}Co δ temperature sensitivity does not follow the ligand field splitting Δ_o. Ramsey's equation relates the ^{59}Co δ inversely to the energy of the first d−d transition of Co(III). It therefore stands to reason that T-dependent changes in Δ_o for systems with weaker ligand field splittings would drive larger temperature dependence for ^{59}Co δ. Yet, **1**−**6** exhibit Δ_o between those typical for O-donor ligand fields (e.g., $Co(acac)_3$) and N-donor ligand fields (like $[Co(en)_3]^{3+}$, en = ethylenediamine), but $\Delta\delta/\Delta T$ for **1**−**6** is lower than both sets of species. Thus, these results provide additional disproof that electronic structure alone is responsible for ^{59}Co $\Delta\delta/\Delta T$. Second, the temperature dependence does not correlate with the C−N or C−S stretching frequencies. Dynamic, temperature-dependent movement of the R groups could potentially influence the C−N bond, and, by induction/resonance, the Co−S interaction, as a mechanism of temperature sensitivity. This work disproves that option as a dominant influence.

Thermal Resolution and Spin Relaxation Mechanisms. The ratio between the temperature sensitivity ($\Delta\delta/\Delta T$) and the full-width half-maximum of the spectral peak ($\nu_{1/2}$, here in ppm) defines the resolution of a temperature sensor as $(\Delta\delta/\Delta T)/\nu_{1/2}$ in units of °C^{-1}. A higher ratio enables greater temperature sensing precision. Using the values for $\Delta\delta/\Delta T$ and $\nu_{1/2}$ obtained in this study, we find resolutions of 0.13, 0.06, 0.04, 0.15, 0.08, and 0.07 °C^{-1} **1**−**6**, respectively, in $CDCl_3$. These values vary slightly, by ca. 0.06 °C^{-1}, as a function of solvent. The resolutions of **1**−**6** are all comparable to ^{1}H NMR thermometers,[3] and in some cases, even slightly higher, despite the larger $\Delta\delta/\Delta T$ for the ^{59}Co nuclei relative to ^{1}H. However, the resolutions fall significantly short of those displayed by $Co(acac)_3$ and $Co(accp)_3$, which are *ca.* 3.66 and 3.18 °C^{-1}, respectively.[11] To the best of our knowledge, **1**−**6** collectively exhibit the lowest resolutions of any ^{59}Co thermometers described in the literature.

We attribute the low resolutions of **1**−**6** to two features: the low $\Delta\delta/\Delta T$ values and the fast spin relaxation that broadens peak line widths. The key question, then, is what the governs that relaxation, as it should have a direct impact on the line width. Note that, since T_2* (lifetime broadening) closely corresponds to T_1 in magnitude and temperature dependence (Figure 5), differences in line widths should track closely with differences in the operative mechanisms of longitudinal relaxation. For ^{59}Co, there are four possible contributing relaxation mechanisms, all associated with rapid molecular tumbling in the extreme narrowing limit: (i) ^{59}Co quadrupolar relaxation,[91] (ii) field-dependent ^{59}Co CSA relaxation, (iii) temperature-dependent spin-rotation relaxation, (iv) and indirect scalar coupling of the second kind.[92,93] The latter two are discarded as major contributors, since increases in T_1 are not proportional to increased temperature and there are no significant J-couplings that could outweigh contributions from the quadrupolar interaction and CSA. We further note that peak broadening was generally higher for samples in high-viscosity solvents (which are not necessarily those with highest polarity; see Figures S16 and Table S23), similar to other studies.[63] Our foregoing data show that these observations *do not* reflect mechanism (iii) but rather the contributions of these solvents to the correlation times for the operative spin relaxation mechanisms.

The majority of our SSNMR data point toward a dominant contribution to relaxation effects from the quadrupolar interaction (QI) and chemical shift anisotropy (CSA). Indeed, the ^{59}Co EFG and CS tensors and the $T_1(^{59}Co)$ relaxation measurements from solution indicate that the quadrupolar relaxation mechanism is dominant in every case, despite the inhomogeneous broadening of the ^{59}Co CT patterns arising from the SOQI and CSA having similar magnitudes. These NMR data therefore suggest that cobalt complexes with reduced values of C_Q but large values of Ω are likely the best candidates for sharp-line width solution-state ^{59}Co NMR thermometers.

Our interpretation of all the collected data points toward a synergy that induces the low thermometer resolutions of **1**−**6**: low $\Delta\delta/\Delta T$ from low q_{Raman} and fast relaxation from high C_Q. We note that T_1 can become long (on the order of seconds) when the geometry is highly octahedral, such as in $[Co(CN)_6]^{3-}$,[94] where a long T_1 (and correspondingly long T_2) enables the line width to be dictated not by relaxation, but by the homogeneity of the magnetic field of the NMR spectrometer. In **1**−**6**, the sharp bite angle of the CS_2−donors and the tris-ligated coordination shell distort the molecule toward an axial, quasi-D_3 symmetry, which raises C_Q and shortens T_1, resulting in significant, quadrupolar-dominated peak broadening.[92]

Potential for Coordination-Number Effects. After reflection, we propose here a design hypothesis toward future high-resolution thermometers that could include heavy-atom donors. First, we note that a six-coordinate environment closer to octahedral geometry would be advantageous to minimize the effect of C_Q on peak broadening. In principle, such a structure can be achieved for Co−S_6 complexes by increasing

https://doi.org/10.1021/acs.inorgchem.4c05385
Inorg. Chem. 2025, 64, 6531−6543

the bite angles of the coordinating bidentate ligands or moving to monodentate ligands.

A second hypothesized future design criterion should address the observed low q_{Raman} (Scheme 1). A cursory investigation of the $3N-6$ vibrational degrees of freedom of the $Co-O_6$ and $Co-S_6$ coordination spheres reveals similar expected numbers of vibrations (15 total, 12 Raman-active) that contribute to $\Delta\delta/\Delta T$. If we instead think about the second coordination shell, specifically, the number of atoms that link the donor atoms, the results differ. For acac-like ligands, which have three atoms linking the O donors, 42 vibrations are expected from that extended coordination shell, 35 of which are Raman active. In contrast, for the dithiocarbamate ligands of **1−6**, only one atom links the S-donor atoms, and therefore the extended coordination shell only has 24 total vibrations, 20 of which are Raman active. Hence, ligands with larger connectivity between the S-donor atoms may raise q_{Raman} enough for higher $\Delta\delta/\Delta T$. Such a result would mimic the results of increased donor-atom connectivity $\Delta\delta/\Delta T$ studies on N-donor Co(III) complexes.[13]

Scheme 1. Proposed Origin of Low Partition Coefficient in 1−6 Compared to Acetylacetonato Complexes and Analogs

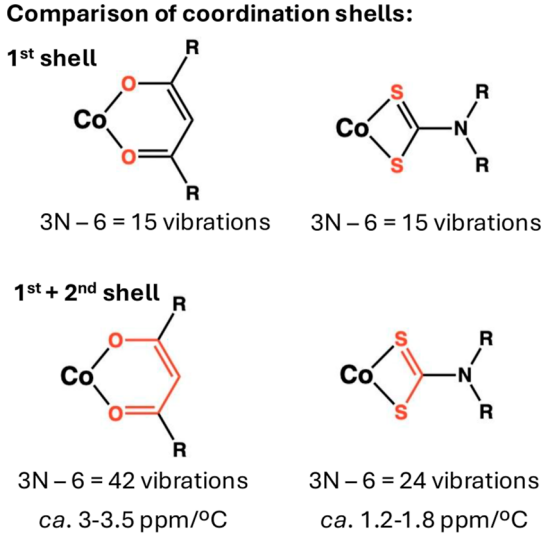

CONCLUSION

In summary, this study represents the first comprehensive examination of the ^{59}Co NMR temperature dependence and SSNMR characteristics of mononuclear $Co-S_6$ complexes. Though the heavier mass of the ligand shell did not simply amplify the temperature sensitivity of the ^{59}Co chemical shift, the results nevertheless support the established link between the vibrational partition function and temperature sensitivity. Furthermore, our data rule out other potential mechanisms for controlling temperature sensitivity, such as ligand dynamics and pure electronic structure considerations. Designing $Co-S_6$ complexes with wider bite angles, similar to $Co(acac)_3$ complexes, could significantly reduce C_Q contributions to NMR relaxation and potentially make a large impact.

The counterintuitive suppression of the vibrational partition function with heavier atoms bears further study. We do not consider the story to be over for heavy-atom donors, because, as described above, there is evidence that unanticipated ligand effects in **1−6** may suppress the effects of the heavy donor atoms. Tests of ligands where the S-donor atoms are linked through diatomic bridges or greater (e.g., an S atom analogue of acac,[95] or cyclic thioethers[96]) are ongoing and the influence of those ligands on ^{59}Co temperature sensitivity will be reported in due course.

ASSOCIATED CONTENT

Supporting Information

The Supporting Information is available free of charge at https://pubs.acs.org/doi/10.1021/acs.inorgchem.4c05385.

Additional characterization, spectral data, and interpretation (PDF)

Accession Codes

Deposition Number 2426923 contains the supplementary crystallographic data for this paper. These data can be obtained free of charge via the joint Cambridge Crystallographic Data Centre (CCDC) and Fachinformationszentrum Karlsruhe Access Structures service.

AUTHOR INFORMATION

Corresponding Authors

Robert W. Schurko − *Department of Chemistry and Biochemistry, Florida State University, Tallahassee, Florida 32306, United States; National High Magnetic Field Laboratory, Tallahassee, Florida 32310, United States*; Email: rschurko@fsu.edu

Joseph M. Zadrozny − *Department of Chemistry and Biochemistry, The Ohio State University, Columbus, Ohio 43210, United States*; orcid.org/0000-0002-1309-6545; Email: zadrozny.13@osu.edu

Authors

Ökten Üngör − *Department of Chemistry and Biochemistry, The Ohio State University, Columbus, Ohio 43210, United States*

Sara Termos − *Department of Chemistry and Biochemistry, Florida State University, Tallahassee, Florida 32306, United States; National High Magnetic Field Laboratory, Tallahassee, Florida 32310, United States*

Complete contact information is available at: https://pubs.acs.org/10.1021/acs.inorgchem.4c05385

Author Contributions

‖Ö.Ü. and S.T. denotes equal authorship. Ö.Ü. executed the syntheses, characterizations, formal analysis, and writing the original draft. S.T. acquired all the solid-state NMR data and analyzed the data to obtain NMR parameters. R.W.S. assisted in the interpretation of the NMR data, graduate research supervision, and acquisition of funding. J.M.Z. was responsible for conceptualization, validation, funding acquisition, supervision, writing—review and editing. All authors were involved in assembling the manuscript.

Notes

The authors declare no competing financial interest.

ACKNOWLEDGMENTS

J.M.Z. and Ö.Ü. acknowledge support by the National Science Foundation (NSF) via a CAREER award (NSF-2047325/2419717). NMR and standard molecular characterization were performed at the Colorado State University Analytical Resources Core Facility RRID: SCR_021758, which is supported by an NIH-SIG award (1S10OD021814-01) and

the CSU-CORES Program. R.W.S. and S.T. thank the Basic Energy Sciences program of the Department of Energy (DE-SC0022310), and also Florida State University, and the National High Magnetic Field Laboratory (NHMFL), which is funded by the National Science Foundation Cooperative Agreement (DMR-1644779, DMR-2128556) and the State of Florida. R.W.S. also acknowledges funding to support early research in this area from the NSF Chemical Measurement and Imaging Program, with partial cofunding from the Solid State and Materials Chemistry Program (NSF-2003854). A portion of this work was performed at the Raman Microspectroscopy Laboratory in the Department of Geological Science at the University of Colorado-Boulder. Finally, we acknowledge Eric Ellison, Dr. Zhehong Gan, and Dr. Fred Mentink-Vigier for experimental assistance and helpful comments.

REFERENCES

(1) Rieke, V.; Butts Pauly, K. MR thermometry. *J. Magn. Reson. Imag.* **2008**, *27* (2), 376−390.
(2) Silletta, E. V.; Jerschow, A.; Madelin, G.; Alon, L. Multinuclear Absolute Magnetic Resonance Thermometry. *Commun. Phys.* **2019**, *2*, 1−10.
(3) Üngör, Ö.; Ozvat, T. M.; Grundy, J. V.; Zadrozny, J. M. Transition Metal NMR Thermometry. *Comprehensive Inorganic Chemistry III*; Elsevier, 2023; pp 745−770.
(4) Winter, L.; Oberacker, E.; Paul, K.; Ji, Y.; Oezerdem, C.; Ghadjar, P.; Thieme, A.; Budach, V.; Wust, P.; Niendorf, T. Magnetic Resonance Thermometry: Methodology, Pitfalls And Practical Solutions. *Int. J. Hyperthermia* **2016**, *32*, 63−75.
(5) Brace, C. Thermal Tumor Ablation In Clinical Use. *IEEE Pulse* **2011**, *2*, 28−38.
(6) Zhu, M.; Sun, Z.; Ng, C. K. Image-Guided Thermal Ablation With MR-Based Thermometry. *Quant. Imag. Med. Surg.* **2017**, *7*, 356−368.
(7) Rzechorzek, N. M.; Thrippleton, M. J.; Chappell, F. M.; Mair, G.; Ercole, A.; Cabeleira, M.; Rhodes, J.; Marshall, I.; O'Neill, J. S.; The CENTER-TBI High Resolution ICU (HR ICU) Sub-Study Participants and Investigators. A daily temperature rhythm in the human brain predicts survival after brain injury. *Brain* **2022**, *145* (6), 2031−2048.
(8) Freeman, R.; Murray, G. R.; Richards, R. E. Cobalt Nuclear Resonance Spectra. *Proc. R. Soc.* **1997**, *242* (1231), 455−466.
(9) Bramley, R.; Brorson, M.; Sargeson, A. M.; Schaeffer, C. E. Cobalt-59 NMR Chemical Shifts Of Cobalt(III) Complexes; Correlations With Parameters Calculated From Ligand-Field Spectra. *J. Am. Chem. Soc.* **1985**, *107*, 2780−2787.
(10) Üngör, Ö.; Ozvat, T. M.; Ni, Z.; Zadrozny, J. M. Record Chemical-Shift Temperature Sensitivity in a Series of Trinuclear Cobalt Complexes. *J. Am. Chem. Soc.* **2022**, *144*, 9132−9137.
(11) Üngör, Ö.; Sanchez, S.; Ozvat, T. M.; Zadrozny, J. M. Asymmetry-enhanced ^{59}Co NMR thermometry in Co(iii) complexes. *Inorg. Chem. Front.* **2023**, *10*, 7064−7072.
(12) Ozvat, T. M.; Johnson, S. H.; Rappe, A. K.; Zadrozny, J. M. Ligand Control of (59)Co Nuclear Spin Relaxation Thermometry. *Magnetochemistry* **2020**, *6* (4), 58−68.
(13) Ozvat, T. M.; Pena, M. E.; Zadrozny, J. M. Influence of ligand encapsulation on cobalt-59 chemical-shift thermometry. *Chem. Sci.* **2019**, *10*, 6727−6734.
(14) Ozvat, T. M.; Rappe, A. K.; Zadrozny, J. M. Isotopomeric Elucidation of the Mechanism of Temperature Sensitivity in (59)Co NMR Molecular Thermometers. *Inorg. Chem.* **2022**, *61* (2), 778−785.
(15) Bond, A. M.; Colton, R.; Moir, J. E.; Page, D. R. Investigations of Mixed-Ligand Cobalt Dithiocarbamate Complexes By Cobalt-59 Nuclear Magnetic Resonance Spectroscopy, Mass Spectrometry, And Electrochemistry. *Inorg. Chem.* **1985**, *24*, 1298−1302.
(16) Bond, A. M.; Colton, R.; Ho, Y.; Moir, J. E.; Page, D. R.; Stott, R. Characterization of pentakis(dithiocarbamato)dicobalt(III) complexes, [Co2(RR'dtc)5]+, and related complexes in dichloromethane using electrochemical and cobalt-59 NMR techniques. *Inorg. Chem.* **1985**, *24* (25), 4402−4407.
(17) Dietzsch, W.; Duffy, N. V.; Katsoulos, G. A.; Olk, B. Multinuclear (1H, 13C, 59Co, 77Se) NMR studies of thioseleno- and diselenocarbamato complexes of cobalt(III) and indium(III) in CDCl3 solution. *Inorg. Chim. Acta* **1991**, *184* (1), 89−97.
(18) Grant, G. J.; Shoup, S. S.; Hadden, C. E.; VanDerveer, D. G. Cobalt(III) complexes of crown thioethers: the crystal structure of (1,4,7,11,14,17-hexathiacycloeicosane) cobalt (III) tetrafluoroborate dihydrate. *Inorg. Chim. Acta* **1998**, *274* (2), 192−200.
(19) Eagle, C. T.; Farrar, D. G.; Holder, G. N.; Gooden, D. M.; Goodman, A. B.; Wyatt, S. W. Synthesis and Characterization of Tris(diethyldithiocarbamato) Cobalt(III) as an Undergraduate Inorganic Laboratory. *Chem. Educ.* **1999**, *4*, 105−107.
(20) Kong, W.; Huang, W.; He, Z.; Ping, J. Preparation of Dialkyl Dithiocarbamate. China Patent CN112341369, 2001.
(21) Biswas, K.; Ghosh, S.; Ghosh, P.; Basu, B. Cyclic Ammonium Salts of Dithiocarbamic Acid: Stable Alternative Reagents For The Synthesis of S-Alkyl Carbodithioates From Organyl Thiocyanates In Water. *J. Sulphur Chem.* **2016**, *37*, 361−376.
(22) Donnici, C. L.; Nogueira, L. J.; Araujo, M. H.; Oliveira, S. R.; Magalhaes, T. F.; Lopes, M. T.; Silva, A.; Ferreira, A. M.; Martins, C. V.; de Resende Stoianoff, M. A. In Vitro Studies of The Activity of Dithiocarbamate Organoruthenium Complexes Against Clinically Relevant Fungal Pathogens. *Molecules* **2014**, *19*, 5402−5420.
(23) Sheldrick, G. M. *SADABS, Software for Empirical Absorption Correction*; University of Göttingen, 1996.
(24) Sheldrick, G. M. Crystal Structure Refinement with SHELXL. *Acta Crystallogr., Sect. C: Struct. Chem.* **2015**, *71*, 3−8.
(25) Sheldrick, G. M. SHELXT - Integrated Space-Group and Crystal-Structure Determination. *Acta Crystallogr., Sect. A* **2015**, *71*, 3−8.
(26) Sheldrick, G. M. A. Short History of SHELX. *Acta Crystallogr.* **2008**, *64*, 112−122.
(27) Medek, A.; Frydman, V.; Frydman, L. Central Transition Nuclear Magnetic Resonance in the Presence of Large Quadrupole Couplings: Cobalt-59 Nuclear Magnetic Resonance of Cobaltophthalocyanines. *J. Phys. Chem. A* **1999**, *103* (25), 4830−4835.
(28) Ooms, K. J.; Terskikh, V. V.; Wasylishen, R. E. Ultrahigh-field solid-state 59Co NMR studies of Co(C2B9H11)2- and Co(C5H5)2+ salts. *J. Am. Chem. Soc.* **2007**, *129* (21), 6704−6795.
(29) Kupce, Ē.; Freeman, R. Stretched Adiabatic Pulses for Broadband Spin Inversion. *J. Magn. Reson.* **1995**, *117* (2), 246−256.
(30) O'Dell, L. A.; Rossini, A. J.; Schurko, R. W. Acquisition of ultra-wideline NMR spectra from quadrupolar nuclei by frequency stepped WURST−QCPMG. *Chem. Phys. Lett.* **2009**, *468* (4−6), 330−335.
(31) O'Dell, L. A.; Schurko, R. W. QCPMG using adiabatic pulses for faster acquisition of ultra-wideline NMR spectra. *Chem. Phys. Lett.* **2008**, *464* (1−3), 97−102.
(32) Koppe, J.; Frerichs, J. E.; Hansen, M. R. Pushing the Detection Limit of Static Wideline NMR Spectroscopy Using Ultrafast Frequency-Swept Pulses. *J. Phys. Chem. Lett.* **2023**, *14* (48), 10748−10753.
(33) Schurko, R. W. Acquisition of Wideline Solid-State NMR Spectra of Quadrupolar Nuclei. In *NMR of Quadrupolar Nuclei in Solid Materials*; Harris, R. K., Wasylishen, R. L., Eds.; eMagRes., 2011.
(34) van Meerten, S. G. J.; Franssen, W. M. J.; Kentgens, A. P. M. ssNake: A cross-platform open-source NMR data processing and fitting application. *J. Magn. Reson.* **2019**, *301*, 56−66.
(35) Perras, F. A.; Paterson, A. L. Automatic fitting of multiple-field solid-state NMR spectra. *Solid State Nucl. Magn. Reson.* **2024**, *131*, 101935.
(36) Brennan, T.; Bernal, I. Crystal and molecular structure of tris(diethyldithiocarbamato)cobalt(III). *J. Phys. Chem.* **1969**, *73* (2), 443−445.
(37) Healy, P. C.; Connor, J. W.; Skelton, B. W.; White, A. H. Alkyl Substituent Effects in Diamagnetic Dithiocarbamate Cobalt(III) and Nickel(II) Complexes. *Aust. J. Chem.* **1990**, *43*, 1083−1095.

https://doi.org/10.1021/acs.inorgchem.4c05385
Inorg. Chem. 2025, 64, 6531−6543

(38) Zhu, H. P.; Deng, Y. H.; Huang, X. Y.; Chen, C. N.; Liu, Q. T. Tris(N,N-diethyldithiocarbamato-S,S')vanadium(III). *Acta Crystallogr., Sect. C: Struct. Chem.* **1997**, *53*, 692−693.
(39) Raston, C. L.; White, A. H. Crystal Structure of Tris(N,N-diethyldithiocarbamato)chromium(III). *Aust. J. Chem.* **1977**, *30*, 2091−2094.
(40) Elliot, R. L.; West, B. O.; Snow, M. R.; Tiekink, E. R. T. A Second Polymorph of tris(N,N-diethyldithiocarbamato)manganese-(III). *Acta Crystallogr., Sect. C: Struct. Chem.* **1986**, *42*, 763−764.
(41) Alvarez, S.; Avnir, D.; Llunell, M.; Pinsky, M. Continuous Symmetry Maps And Shape Classification. The Case of Six-Coordinated Metal Compounds. *New J. Chem.* **2002**, *26* (8), 996−1009.
(42) Alvarez, S.; Alemany, P.; Casanova, D.; Cirera, J.; Llunell, M.; Avnir, D. Shape Maps and Polyhedral Interconversion Paths In Transition Metal Chemistry. *Coord. Chem. Rev.* **2005**, *249* (17−18), 1693−1708.
(43) Sonia, A. S.; Bhaskaran, R. Tris Dithiocarbamate of Co(III) Complexes: Synthesis, Characterization, Thermal Decomposition Studies And Experimental And Theoretical Studies On Their Crystal Structures. *J. Mol. Struct.* **2017**, *1134*, 416−425.
(44) Halls, D. J. The properties of dithiocarbamates A Review. *Mikrochim. Acta* **1969**, *57* (1), 62−77.
(45) Margotrigiano, G.; Pellagani, G. C.; Preti, C.; Tosi, G. Dithiocarbamate Complexes of Rhodium(III), Iridium(III), Palladium(II) and Platinum(II). *Bull. Chem. Soc. Jpn.* **1975**, *48*, 1018−1020.
(46) Ajibade, P. A.; Paca, A. M. Tris(Dithiocarbamato)Iron(III) Complexes As Precursors For Iron Sulfide Nanocrystals And Iron Sulfide-Hydroxyethyl Cellulose Composites. *J. Sulphur Chem.* **2019**, *40*, 52−64.
(47) Rajasekharan, M. V.; Chandramouli, G. V. R.; Manoharan, P. T. Polarized Electronic Spectral Studies On Some Diethyldithiocarbamate Complexes of Ni(II) and Pd(II). *Chem. Phys. Lett.* **1989**, *162*, 110−116.
(48) Ramalingam, K.; Aravamudan, G.; Seshasayee, M. Cyclic Voltammetric and Infrared Spectral Studies on the Interaction of Ni(II) Dithiocarbamates with Triphenylphosphine and the Crystal and Molecular Structure of Diethyldithiocarbamatobis-(triphenylphosphine)nickel(II)perchlorate, [Ni(dedtc)(PPh3)2]-ClO4. *Inorg. Chim. Acta* **1987**, *128* (2), 231−237.
(49) Gurumoorthy, G. Synthesis and Characterization of Cobalt-(III)dithiocarbamate Complexes. *Malaya J. Matematik* **2020**, *S*, 2200−2203.
(50) Odularu, A. T.; Ajibade, P. A. Dithiocarbamates: Challenges, Control, and Approaches to Excellent Yield, Characterization, and Their Biological Applications. *Bioinorg. Chem. Appl.* **2019**, *2019*, 1−15.
(51) Yamasaki, A.; Yajima, F.; Fujiwara, S. Nuclear Magnetic Resonance Studies On Cobalt Complexes. I. Cobalt-59 Nuclear Magnetic Resonance Spectra of Cobalt(III) Complexes. *Inorg. Chim. Acta* **1968**, *2*, 39−42.
(52) Fujiwara, S.; Yajima, F.; Yamasaki, A. NMR Studies of Cobalt Complexes. Theoretical Interpretation of Cobalt-59 Chemical Shifts. *J. Magn. Reson.* **1969**, *1*, 203−210.
(53) Martin, R. L.; White, A. H. Cobalt-59 Nuclear Magnetic Resonance of Sulphur, Selenium and Arsenic Chelates of Cobalt (III). *Nature* **1969**, *223*, 394−396.
(54) Kanakubo, M.; Uda, T.; Ikeuchi, H.; Satô, G. P. Solvent and Temperature Dependence of 59Co NMR Chemical Shifts of Tris(acetylacetonato)cobaIt(III) and Tris(dipivaloylmethanato)-cobalt(III). *J. Solution Chem.* **1998**, *27*, 645−653.
(55) Smallwood, I. *Handbook of Organic Solvent Properties*; Butterworth-Heinemann, 1996.
(56) Katritzky, A. R.; Fara, D. C.; Yang, H.; Tamm, K.; Tamm, T.; Karelson, M. Quantitative measures of solvent polarity. *Chem. Rev.* **2004**, *104* (1), 175−198.
(57) Wasylishen, R. L. NMR Relaxation and Dynamics. In *NMR Spectroscopy Techniques*; Bruch, M. D., Ed.; CRC Press, 1996; pp 105−144.
(58) Kirby, C. W.; Puranda, C. M.; Power, W. P. Cobalt-59 Nuclear Magnetic Relaxation Studies of Aqueous Octahedral Cobalt(III) Complexes. *J. Phys. Chem.* **1996**, *100* (35), 14618−14624.
(59) Chan, J. C. C.; Au-Yeung, S. C. F. Cobalt-59 NMR spectroscopy. *Annu. Rep. NMR Spectrosc.* **2000**, *41*, 1−54.
(60) Knop, O.; Palmer, E. M.; Robinson, R. W. Arrangements of point charges having zero electric-field gradient. *Acta Crystallogr., Sect. A* **1975**, *31* (1), 19−31.
(61) Akitt, J. W.; McDonald, W. S. Arrangements of ligands giving low electric field gradients. *J. Magn. Reson.* **1984**, *58* (3), 401−412.
(62) Kirby, C. W.; Power, W. P. Cobalt-59 chemical shift and quadrupolar tensors of simple octahedral cobalt(III) complexes. *Can. J. Chem.* **2001**, *79* (3), 296−303.
(63) Kanakubo, M.; Inoue, N.; Ikeuchi, H.; Satô, G. P. Rotational Correlation Times of Tris(acetylacetonato)cobalt(III) in Various Organic Solvents by NMR Relaxation Measurements. *J. Solution Chem.* **2023**, *52* (10), 1117−1128.
(64) Kentgens, A. P. M. A practical guide to solid-state NMR of half-integer quadrupolar nuclei with some applications to disordered systems. *Geoderma* **1997**, *80* (3), 271−306.
(65) Altenhof, A. R.; Gan, Z.; Schurko, R. W. Reducing the effects of weak homonuclear dipolar coupling with CPMG pulse sequences for static and spinning solids. *J. Magn. Reson.* **2022**, *337*, 107174.
(66) Bodart, P. R.; Amoureux, J.-P.; Dumazy, Y.; Lefort, R. Theoretical and experimental study of quadrupolar echoes for half-integer spins in static solid-state NMR. *Mol. Phys.* **2000**, *98* (19), 1545−1551.
(67) Kimball, J. J.; Altenhof, A. R.; Jaroszewicz, M. J.; Schurko, R. W. Broadband Cross-Polarization to Half-Integer Quadrupolar Nuclei: Wideline Static NMR Spectroscopy. *J. Phys. Chem. A* **2023**, *127* (45), 9621−9634.
(68) Hung, I.; Altenhof, A. R.; Schurko, R. W.; Bryce, D. L.; Han, O. H.; Gan, Z. Field-stepped ultra-wideline NMR at up to 36 T: On the inequivalence between field and frequency stepping. *Magn. Reson. Chem.* **2021**, *59* (9−10), 951−960.
(69) Altenhof, A. R.; Jaroszewicz, M. J.; Lindquist, A. W.; Foster, L. D. D.; Veinberg, S. L.; Schurko, R. W. Practical Aspects of Recording Ultra-Wideline NMR Patterns under Magic-Angle Spinning Conditions. *J. Phys. Chem. C* **2020**, *124* (27), 14730−14744.
(70) Koppe, J.; Hansen, M. R. Minimizing Lineshape Distortions in Static Ultra-wideline Nuclear Magnetic Resonance of Half-Integer Spin Quadrupolar Nuclei. *J. Phys. Chem. A* **2020**, *124* (21), 4314−4321.
(71) Pathmalingam, T.; Habib, F.; Widdifield, C. M.; Loiseau, F.; Burchell, T. J.; Gorelsky, S. I.; Beauchemin, A. M.; Bryce, D. L.; Murugesu, M. Combining oximes with azides to create a novel 1-D [NaCoIII2] system: synthesis, structure and solid-state NMR. *Dalton Trans.* **2010**, *39* (6), 1504−1510.
(72) Grahn, H.; Edlund, U.; Holak, T. A. A 59Co NMR chemical shift and relaxation study of preferential solvation toward tris-(acetylacetonato)cobalt(III). *Magn. Reson. Chem.* **1987**, *25* (6), 497−502.
(73) Socol, S. M.; Lacelle, S.; Verkade, J. G. Effect of ligand geometry on cobalt-59 NMR relaxation in hexakis(phosphite)cobalt-(III) complexes. *Inorg. Chem.* **1987**, *26* (19), 3221−3224.
(74) Braunstein, P.; Rose, J.; Granger, P.; Raya, J.; Bouaoud, S. E.; Grandjean, D. Cobalt-59 NMR study of cluster reactions: solvent and ligand effects in mixed-metal, tetrahedral MCo_3 (M = iron, ruthenium) carbonyl clusters. Crystal structure of $FeCo_3(\mu_3\text{-}H)(\mu\text{-}CO)_3(CO)_8(PPh_2H)$. *Organometallics* **1991**, *10* (10), 3686−3693.
(75) Sizun, C.; Kempgens, P.; Raya, J.; Elbayed, K.; Granger, P.; Rosé, J. ^{59}Co-NMR spectroscopy of the tetrahedral cluster $Co_4(CO)_{12}$: relaxation and exchange. *J. Organomet. Chem.* **2000**, *604* (1), 27−33.
(76) Kempgens, P.; Hirschinger, J.; Elbayed, K.; Raya, J.; Granger, P.; Rosé, J. Multinuclear NMR Study of $HFeCo_3(CO)_9[P(OCH_3)_3]_3$

https://doi.org/10.1021/acs.inorgchem.4c05385
Inorg. Chem. 2025, 64, 6531−6543

in the Solid State and in Solution. *J. Phys. Chem.* **1996**, *100* (6), 2045−2052.
(77) Kanakubo, M.; Ikeuchi, H.; Sato, G. P. Concentration Dependence of Cobalt-59 Longitudinal Relaxation Times of Tris-(acetylacetonato)cobalt(III) in Acetonitrile. *J. Magn. Reson.* **1995**, *112* (1), 13−16.
(78) Kanakubo, M.; Inoue, N.; Ikeuchi, H.; Satô, G. P. Rotational Correlation Times of Tris(acetylacetonato)cobalt(III) in Various Organic Solvents by NMR Relaxation Measurements. *J. Solution Chem.* **2023**, *52* (10), 1117−1128.
(79) Kanakubo, M.; Nozaki, K.; Inoue, N.; Ikeuchi, H.; Satô, G. P. Cobalt-59 NMR relaxation times of symmetric tris(γ-substituted-acetylacetonato)cobalt(III) complexes in benzene. *Inorg. Chim. Acta* **2024**, *561*, 121847.
(80) Dote, J. L.; Kivelson, D.; Schwartz, R. N. A molecular quasi-hydrodynamic free-space model for molecular rotational relaxation in liquids. *J. Phys. Chem.* **1981**, *85* (15), 2169−2180.
(81) Granger, P.; Richert, T.; Elbayed, K.; Kempgens, P.; Hirschinger, J.; Raya, J. Microdynamic motion of tetrahedral clusters studied by 59Co and 99Ru NMR relaxations. *Mol. Phys.* **1997**, *92* (5), 895−902.
(82) Ikeuchi, H.; Kanakubo, M.; Okuno, S.; Sato, R.; Fujita, K.; Hamada, M.; Shoda, N.; Fukui, K.; Okada, K.; Kanazawa, H.; et al. Densities and Viscosities of Tris(acetylacetonato)cobalt(III) Complex Solutions in Various Solvents. *J. Sol. Chem.* **2010**, *39* (10), 1428−1453.
(83) Wang, P.-L.; Hwang, L.-P. Nuclear magnetic resonance relaxation studies on the preferential solvation of tris-acetylacetonato−chromium(III) in bromoform−carbon tetrachloride solutions. *J. Chem. Soc., Faraday Trans. 1* **1989**, *85* (8), 2335−2345.
(84) Steinbach, J. F.; Burns, J. H. Chloroform-bearing Chelates. *J. Am. Chem. Soc.* **1958**, *80* (8), 1839−1841.
(85) Bolagam, R.; Um, S. Hydrothermal Synthesis of Cobalt Ruthenium Sulfides as Promising Pseudocapacitor Electrode Materials. *Coatings* **2020**, *10* (3), 200−215.
(86) Liu, G.; Fang, Q.; Xu, W.; Chen, H.; Wang, C. Vibration assignment of carbon-sulfur bond in 2-thione-1,3-dithiole-4,5-dithiolate derivatives. *Spectrochim. Acta Part A Mol. Spectrosc.* **2004**, *60* (3), 541−550.
(87) Ma, D.; Hu, B.; Wu, W.; Liu, X.; Zai, J.; Shu, C.; Tadesse Tsega, T.; Chen, L.; Qian, X.; Liu, T. L. Highly active nanostructured CoS2/CoS heterojunction electrocatalysts for aqueous polysulfide/iodide redox flow batteries. *Nat. Commun.* **2019**, *10* (1), 1−8.
(88) Bauer, G.; Nikolov, G. S.; Trendafilova, N. Molecular structure and vibrational spectra of bis-N,N'-diethyldithiocarbamate compounds with closed-shell metal ions. *J. Mol. Struct.* **1997**, *415* (1−2), 123−134.
(89) Trendafilova, N. S.; Kellner, R.; Nikolov, G. S. Normal coordinate analysis of the dithiocarbamate ligand and bis-(N,N-diethyldithiocarbamate)nickel(II), copper(II), zinc(II) and cadmium-(II). *J. Mol. Struct.* **1984**, *115*, 439−442.
(90) Nikolov, G. S. Effect of The Bite Angle On The Orbital Energies And The Electronic Spectra of Planar Chelate Coordination Compounds. *J. Inorg. Nucl. Chem.* **1977**, *39*, 249−253.
(91) Bruch, M. *NMR Spectroscopy Techniques*; CRC Press, 1996.
(92) Doddrell, D. M.; Bendall, M. R.; Healy, P. C.; Smith, G.; Kennard, C. H. L.; Raston, C. L.; White, A. H. 59Co and 13C Nuclear Spin Relaxation Studies in Solutions of Symmetric, Bidentate Cobalt(III) Complexes. On the Mechanism of 59Co Spin Relaxation. Crystal Structure Determination of Tris(tropolonato)cobalt(III). *Aust. J. Chem.* **1979**, *32* (6), 1219.
(93) Rose, K. D.; Bryant, R. G. Nuclear magnetic resonance relaxation in symmetrical cobalt(III) complexes. *Inorg. Chem.* **1979**, *18* (5), 1332−1335.
(94) Ader, R.; Loewenstein, A. Nuclear Magnetic Relaxation Studies in Solutions of Symmetric Cobalt (III) Complexes. *J. Magn. Reson.* **1971**, *5* (2), 248−261.
(95) Boyd, P. D. W.; Hope, J.; Martin, R. L. Synthesis and properties of tris(dithioacetylacetonato)vanadium(III). *J. Chem. Soc., Dalton Trans.* **1986**, No. 4, 887−889.
(96) Murray, S. G.; Hartley, F. R. Coordination chemistry of thioethers, selenoethers, and telluroethers in transition-metal complexes. *Chem. Rev.* **1981**, *81* (4), 365−414.

https://doi.org/10.1021/acs.inorgchem.4c05385
Inorg. Chem. 2025, 64, 6531−6543